Journal of Materials Chemistry A

Accepted Manuscript

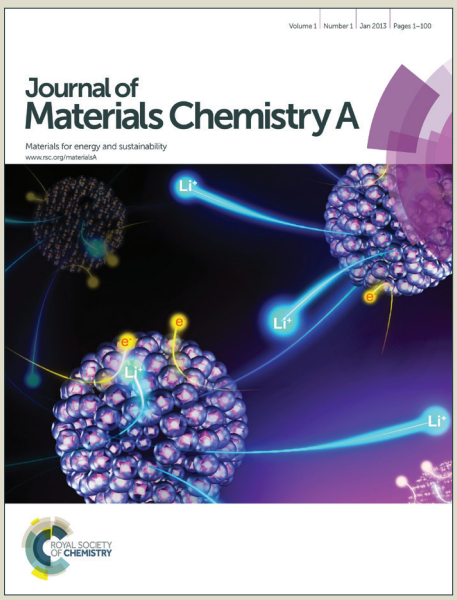

ROYAL SOCIETY OF CHEMISTRY

www.rsc.org/materialsA

Journal of Materials Chemistry A RSC Publishing

ARTICLE

Three-Dimensional Graphene-Co_3O_4 Cathodes for Rechargeable Li-O_2 Batteries

Cite this: DOI: 10.1039/x0xx00000x

Jiakai Zhang, [a] Pengfa Li, [a] Zhenhua Wang, [a] Jinshuo Qiao, [a] David Rooney, [a] Wang Sun*[a] and Kening Sun*[a]

Received 00th January 2014,
Accepted 00th January 2014

DOI: 10.1039/x0xx00000x

www.rsc.org/

A three-dimensional (3D) graphene-Co_3O_4 electrode was prepared through a two-step method in which graphene was initially deposited on a Ni foam with Co_3O_4 then grown on the resulting graphene structure. Cross-linked Co_3O_4 nanosheets with an open pore structure were fully and vertically distributed through the graphene skeleton. The free-standing and binder-free monolithic electrode was used directly as a cathode in a Li-O_2 battery. This composite structure exhibited enhanced performance with a specific capacity of 2453 mAh g^{-1} at 0.1 mA cm^{-2} and 62 stable cycles with 583 mAh g^{-1} (1000 mAh g_{carbon}^{-1}). The excellent electrochemical performance is associated with the unique architecture and superior catalytic activity of the 3D electrode.

Introduction

With increasing demand for high-energy-density storage systems, Li-O_2 batteries have triggered worldwide and strong interest as novel and superior rechargeable batteries. Li-O_2 batteries can deliver substantially higher energy density (~11700 Wh kg^{-1}) when compared with other chemical batteries, such as conventional Li-ion batteries.[1-5] Abandoning the requirements for certain chemicals inside the cell and allowing lithium to react directly with O_2 from the air at a porous electrode increases the capacity remarkably. However, Li-O_2 batteries are still in their developmental infancy and at present the energy density of such Li-O_2 batteries fails to reach the theoretical value in practical applications. Other limitations of this complex system, such as poor cyclability and low round-trip efficiency, still need to be studied in detail.[6-9] Among all the factors that strongly influence the capacity and the cycle efficiency, the catalyst used is considered by many to be key.[10-13]

Previous studies have suggested that the use of active catalysts could accelerate the generally sluggish kinetics of the oxygen reduction reaction (ORR) during discharging and the oxygen evolution reaction (OER) during charging.[14,15] A great deal of effort has therefore been devoted to exploring the design and synthesis of efficient catalysts for Li-O_2 batteries, including noble metals,[16,17] carbon materials[18-21] and transition metal oxides.[22-25] Bruce *et al.* reported that a dissolved catalyst, tetrathiafulvalene (TTF), also considered as redox mediator, delivered complete reversibility of Li_2O_2 formation/decomposition for 100 cycles, and the charge voltage is less than 3.5 V.[26] Their work provides a distinctive method to improve the performance of Li-O_2 cell, but it does not upgrade immobilized catalyst essentially.

Among the various oxide catalysts studied, Co_3O_4 has been considered to be a promising electroactive material with great potential in view of its low cost, high redox activity, and environmental friendliness. For example Bruce *et al.* showed that Co_3O_4 exhibited the best combination between a high first discharge capacity and capacity retention on cycling.[27] Previously reported Co_3O_4-based electrodes for Li-O_2 batteries have been produced by traditional slurry-coating technology.[28,29] Using this method the catalyst may not be dispersed uniformly on the support and using organic binders is thought to promote degradation of the Li-O_2 battery as a result of binder-related side-effects.[30] Wang *et al.* presented a binder-free Ru/$TiSi_2$ electrode system using gas phase preparation method, and the cathode permits Li−O_2 operations for over 100 cycles with average round-trip efficiencies >70%. However, taking into account the high cost of the noble metal, inexpensive alternatives have to be considered.[31]Therefore, novel and binder-free electrodes, which result in electroactive Co_3O_4 being in direct and better electric contact with substrates are highly desirable to avoid aforementioned problems that plague electrochemical performance. To date several researches have focused on designing binder-free electrodes for Li-O_2 batteries and these have been shown to yield high capacities and cycle performance.[32,33]

In addition to the use of catalyst promoters it is also known that graphene presents great promise in the development of new systems due to its extraordinary electronic conductivity, and ultra large specific surface area.[34-36] Many approaches

have been explored to fabricate graphene-based nanocomposites for energy-related applications.[37-40] Compared with chemically reduced graphene oxide (rGO),[41,42] the chemical vapour deposition (CVD)-synthesized graphene foams are seamlessly continuous and highly conductive due to the low fraction of surface defects.[43-48]

In this work, we report the fabrication of a binder-free air electrode consisting of a three-dimensional (3D) graphene-Co_3O_4 structure using a two-step method. Firstly, 3D graphene was deposited on a Ni foam by CVD. Subsequently Co_3O_4 nanosheets were grown on the graphene through a hydrothermal reaction. To the best of our knowledge, this is the first study reporting a 3D graphene-Co_3O_4 electrode with this approach for Li-O_2 batteries. Fig. 1 illustrates the overall fabrication process of the composite electrode. This obtained 3D graphene-Co_3O_4 could be directly used as the O_2 cathode, and demonstrates enhanced performance in a Li-O_2 battery.

As a free-standing monolithic electrode without any polymer binder, this approach holds many tailored advantages: (1) Co_3O_4 assembled by uniform and cross-linked nanosheets grows directly on graphene, which inherits the interconnected 3D scaffold of the Ni foam thus favouring oxygen transport and electrolyte penetration; (2) Compared with conventional paste coating methods the direct contact, without the need for a binder, of Co_3O_4 nanosheets with the highly conductive graphene could facilitate continuous and high electron transfer flux throughout the cathode; (3) The open macropores between the Co_3O_4 nanosheets offers sufficient channels and abundant catalytic sites.

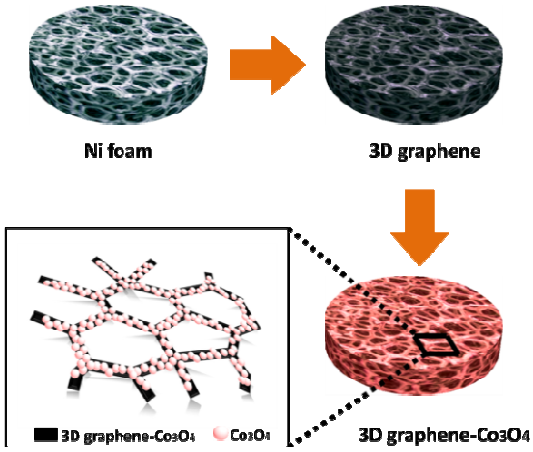

Fig. 1 Schematic of the synthetic procedure used to obtain the 3D graphene-Co_3O_4 nanocomposite.

Experimental

Synthesis of 3D Graphene

Ni foam (320 g m^{-2} with a thickness of 1.2 mm) was cut into pieces of 12 mm radius and cleaned in 3M HCl solution, ethanol and then deionized water for 15 min, respectively. The treated Ni foam was then placed in the centre of a quartz tube, followed by heating to 1000 °C within 3 hours in a horizontal tube furnace under Ar (200 s.c.c.m.) and H_2 (40 s.c.c.m.) after which it was held at 1000 °C for 10 min in order to clean the surface. Ethanol was then introduced into the tube under the Ar/H_2 flow and atmospheric pressure at 1000 °C to grow graphene on the Ni foam skeleton. After reaction for 10 min, the furnace was quickly cooled to room temperature at a cooling rate of >200 °C/min while still under the Ar/H_2 atmosphere by quickly removing it from the hot-zone of the furnace. The loading of graphene was measured by micro-balance with an accuracy of 0.01 mg. The weight of graphene on each Ni foam was around 0.7 mg.

Synthesis of Co_3O_4 nanosheets on 3D graphene

Herein we employed an ammonia-evaporation-induced method to facilitate the growth of the Co_3O_4 catalyst on the 3D graphene structure. 30 mmol $Co(NO_3)_2{\cdot}6H_2O$ and 10 mmol $(NH_4)_2SO_4$ were dissolved in 70 mL of H_2O, then 45 mL of ammonia solution was slowly added with vigorous magnetic stirring. The mixture, after being magnetically stirred for another 10 min, was transferred to an incompletely covered glass bottle. The 3D grapheme electrode was immersed in the reaction solution with growth of the Co_3O_4 occurring at 90 °C for 3 h, 6 h and 9 h. The electrode was then removed, washed with distilled water repeatedly and dried at 60 °C for 2h. This was followed by calcination at 300 °C for 3 h under Ar. On average, approximately 0.4 mg, 0.5 mg and 0.7 mg of Co_3O_4 nanosheets were grown on each 3D graphene electrode, corresponding to different time of 3 h, 6 h and 9 h for growing Co_3O_4, respectively.

Characterisation

The morphology was characterised using a scanning electron microscope (SEM, QUANTA FEG 250) and high resolution transmission electron microscope (HRTEM, JEOL JEM 2010). The obtained products were characterized by X-ray diffraction (XRD, Rigaku Ultima IV, Cu Kα radiation, 40KV, 40 mA). X-ray photoelectron spectroscopy (XPS) was carried out on Physical Electronics 5400 ESCA. The specific surface area and pore size distribution were determined by N_2 adsorption-desorption measurements (Quantachrome Instrument ASIQM0VH002-5). Raman was also performed on a Renishaw RM 2000 using a 633 nm laser.

Electrochemical measurements

The 2025-type coin cells were assembled in an argon-filled glove box (MBRAUN, H_2O< 0.5 ppm, O_2< 0.5 ppm). Cell pans were machine drilled with 7 × Φ 1.0 mm holes in an evenly distributed pattern for oxygen access. Free-standing 3D graphene-Co_3O_4 and 3D graphene served as the cathode directly while pure lithium metal was used as the anode, a glass filter (Whatman grade GF/D) was employed as a

separator and 1 M $LiCF_3SO_3$ in tetraethylene glycol dimethyl ether (TEGDME) was used as the electrolyte. The galvanostatic discharge-charge measurements were performed on battery test system (LAND CT2001A) between 2.0 and 4.3 V (*vs.* Li^+/Li) at different rates at room temperature. The specific capacity was calculated based on the total amount of graphene and Co_3O_4 if not specified. Cyclic voltammetry (CV) experiments were conducted at a scan rate of 0.1 mV s^{-1} between 2.0 and 4.5 V *vs.* Li^+/Li on a CHI 660D (Shanghai Chenhua Instrument). Electrochemical impedance spectroscopy (EIS) was performed on a PARSTAT 2273 at a frequency range from 100 kHz to 10 mHz with an AC voltage amplitude of 5 mV.

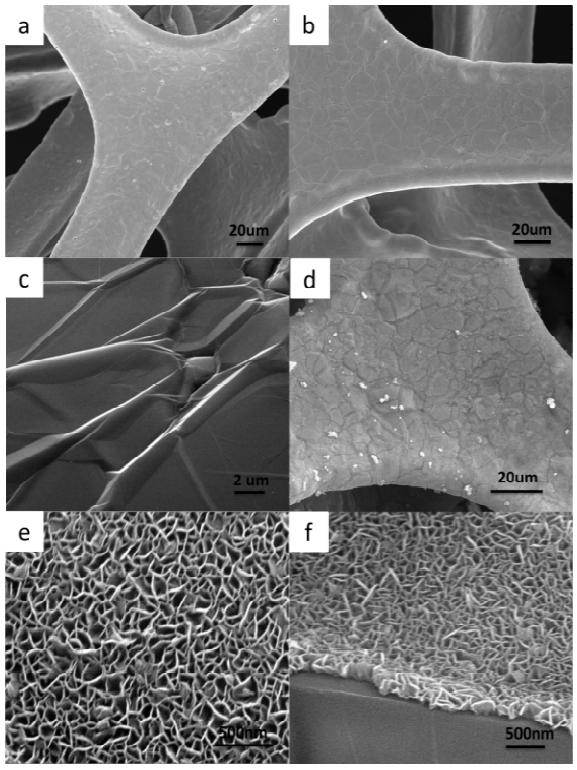

Fig. 2 SEM images of (a) initial Ni foam; (b, c) 3D graphene at different magnifications; (d, e, f) 3D graphene-Co_3O_4 at different magnifications. The hybrid electrode was prepared with 6 h growing time of Co_3O_4.

Results and discussion

The microstructure of the Ni foam, 3D graphene and 3D graphene-Co_3O_4 were examined using scanning electron microscopy (SEM). A porous Ni foam, with an interconnected 3D scaffold (Fig. 2a), was used as a template for the growth of graphene. Graphene was coated on the surface of the Ni foam by the CVD (Fig. 2b and 2c). The images indicate that wrinkles and ripples were clearly formed on the graphene films, which are attributed here to the different thermal expansion coefficients of nickel and graphene.[44] Following hydrothermal treatment, the graphene skeleton is almost fully and uniformly covered by the network of Co_3O_4 nanosheets (Fig. 2d). It is likely that the wrinkles and ripples result in better mechanical interlocking and consequently improved adhesion, which ensures the formation of a free-standing structure and favourable low-resistance pathway for electron transfer. The different growing time of Co_3O_4 nanosheets affect the morphology and thickness of product (Fig. S1). For the 3D graphene-Co_3O_4 composite, the growing Co_3O_4 sheets for 6 h are interconnected with each other, exhibiting an open pore structure, as shown in Fig. 2e. The cross section of Co_3O_4 layer is revealed in Fig. 2f, indicating that the thickness of Co_3O_4 on the substrates is about 150 nm. The Co_3O_4 nanosheets vertically aligned to the graphene not only possesses good conductivities due to the shortest pathway in the through-thickness direction, but can facilitate oxygen and electrolyte transportation efficiently. In addition, the electrode without the need for binder can exclude several binder-related side-effects.[30]

The transmission electron microscopy (TEM) image shows that numerous mesopores with sizes about 5-10 nm are distributed in the nanosheets which are composed of plentiful interconnected nanoparticles (Fig. 3a). High-resolution TEM

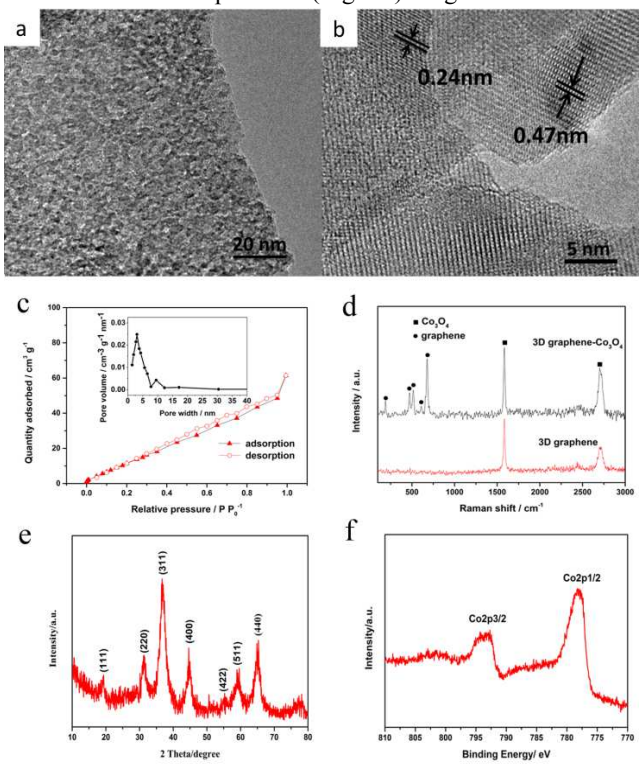

Fig. 3 (a) TEM and (b) HRTEM images of 3D graphene-Co_3O_4 (c) N_2 adsorption-desorption isotherms, and inset is the pore-size distribution of 3D graphene-Co_3O_4 electrode (d) Raman spectra of 3D graphene and 3D graphene-Co_3O_4 composite (e) XRD pattern of Co_3O_4. (f) Co 2p XPS spectra of 3D graphene-Co_3O_4 composite. The hybrid electrode was prepared with 6 h growing time of Co_3O_4.

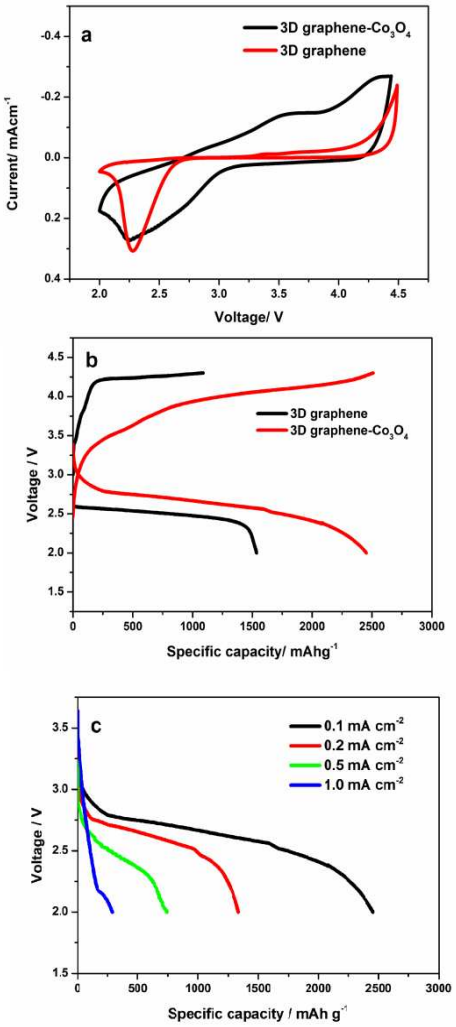

Fig.4 (a) CV curves between 2.0 and 4.5 V at 0.1 mV s^{-1} (b) Discharge-charge curves at a current density of 0.1 mA cm^{-2} for a Li-O_2 battery with a 3D graphene electrode and a 3D graphene-Co_3O_4 electrode (c) the rate performance of Li-O_2 batteries with 3D graphene-Co_3O_4 electrode. The hybrid electrode was prepared with 6 h growing time of Co_3O_4.

(HRTEM) images confirm that the Co_3O_4 nanocrystals have a good crystalline structure (Fig. 3b). It is revealed that the lattice spacings of Co_3O_4 nanocrystals are 0.24 and 0.47 nm, which match well with the lattice spacings of the (311) planes and (111) planes, respectively. The electrode was further characterized by using N_2 adsorption-desorption experiments. The Brunauer-Emmett-Teller (BET) surface area of the 3D graphene-Co_3O_4 electrode with different growing time was recorded in Table S1. The electrode with 6 h growing time exhibited the maximum specific surface area, estimated to be 72.05 m^2 g^{-1}, corresponding to the maximum active sites apparently(Fig. 3c). The pore-size-distribution curve in the inset shows that the pores in the hybrid electrode are mainly mesoporous with a range of 3-10 nm, which is in good agreement with the TEM result. Such structures may be attributed to the ammonia-evaporation-induced method and the subsequent calcination process.[49]

Raman spectra of the 3D graphene and 3D graphene-Co_3O_4 composite demonstrate the existence of both excellent graphene and well-crystallized Co_3O_4. Fig. 3d shows that the characteristic G band at ~1575 cm^{-1} and the 2D band at ~2740 cm^{-1} from graphene were observed. High quality graphene results in an unconspicuous D band at ~1350 cm^{-1}, which is the characteristic peak of the C-C lattice imperfection.[43] Furthermore, five characteristic peaks from Co_3O_4 located at 189, 471, 514, 606 and 678 cm^{-1} correspond, respectively, to 3 F2 g, 1 Eg, and 1 A1 g Raman active modes of the Co_3O_4 nanocrystals.[50, 51] The evidence of Co_3O_4 is also provided by X- ray diffraction (XRD) and X-ray photoelectron spectroscopy (XPS). In the XRD patterns (Fig. 3e), seven obvious diffraction peaks, coincide with the (111), (220), (311), (400), (422), (511), and (440) planes in the standard Co_3O_4 spectrum (JCPDS 43-1003). The Co 2P XPS spectrum shows two major peaks with binding energies at 779.8 and 795.0 eV (Fig. 3f), corresponding to Co 2P3/2 and Co 2P1/2, respectively, with a spin-energy separation of 15.2 eV, which is characteristic of a Co_3O_4 phase,[52] further confirming that the cobalt exists in the Co_3O_4 form.

The electrocatalytic activity of the 3D graphene-Co_3O_4 electrode was investigated by Cyclic Voltammetry (CV) (Fig. 4a). Compared with the 3D graphene electrode without Co_3O_4 (2.7 V), the 3D graphene-Co_3O_4 electrode exhibits a higher ORR onset potential (~3.1 V), which implies a lower ORR kinetic overpotential. However, it is noticed that the peak current of the 3D graphene electrode is slightly higher than that of the 3D graphene-Co_3O_4 electrode. This may be related to the fact that the conductivity of 3D graphene electrode is superior on account of the absence of poorly conductive metal oxides. During anodic scans (> 3 V), the decomposition voltage of discharge products starts earlier and the current density is much more considerable for the 3D graphene-Co_3O_4. These findings indicate that the 3D graphene-Co_3O_4 electrode is obviously more efficient at catalysing the discharge products than the 3D graphene electrode.

In Fig. 4b, the first galvanostatic charge-discharge profile for 3D graphene-Co_3O_4 is compared to basic 3D graphene at a current density of 0.1 mA cm^{-2}. The battery with the 3D graphene-Co_3O_4 cathode exhibits a higher discharge capacity *i.e.* 2453 mAh g^{-1} compared with 1535.7 mAh g^{-1} for the 3D graphene. Another important point is that the hybrid electrode exhibits a discharge plateau between 2.5-2.8 V, about 200 mV higher than that of the electrode without Co_3O_4, and moreover, the charge overpotential was reduced by 350mV. The variation of charging potential with and without Co_3O_4 is more obvious compared with the difference of the discharge voltage, probably because the discharge voltage is closer to the thermodynamic potential (2.96 V). Another possible reason is that mechanism of the charging process depends more on the nature of the catalyst.[27] Obviously, the higher catalytic activity of graphene-Co_3O_4 hybrid relative to

graphene should be responsible for the enlarged capacity and low polarization of 3D graphene-Co_3O_4.

Fig. 4c shows the discharge-charge curves of Li-O_2 cells with 3D graphene-Co_3O_4 cathodes at different current densities. The specific capacity decreases with the progressively increasing current from 0.1 mA cm^{-2} to 1.0 mA cm^{-2}. Remarkably, the discharge capacity at a high current density of 0.5 mA cm^{-2} can still reach 743 mAh g^{-1}. It is noticed that the two-step characteristic was obviously observed at 0.1 and 0.2 mA cm^{-2}, which should be closely related to the hierarchical porous structures.[53] The macropores in sizes of hundreds of nanometers are distributed throughout the network of Co_3O_4 nanosheets while the mesopores of sizes in the range 3-10 nm exist in the flakes as suggested by the pore distribution curves. The varied overpotentials in discharge processes can result from different O_2 diffusion rates, which are in turn related to the different pore size of macropores and mesopores.

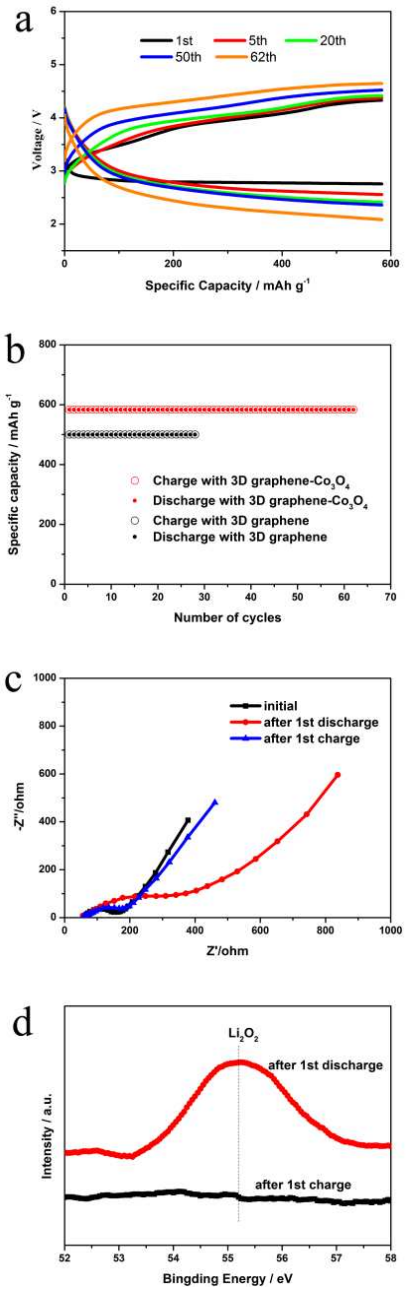

Fig.5 (a) Voltage profiles and cycle performance of Li-O_2 batteries with 3D graphene-Co_3O_4 electrode, (b)Cycle performance of Li-O_2 batteries with 3D graphene electrode and with 3D graphene-Co_3O_4 electrode, (c) Electrochemical impedance spectra of Li-O_2 batteries with 3D graphene-Co_3O_4 electrode, (d) Li 1s XPS of the 3D graphene-Co_3O_4 electrode after discharge-charge processes. The hybrid electrode was prepared with 6 h growing time of Co_3O_4.

Following the capacity-limited cycle approach and to avoid a large depth of discharge, Fig. 5a displays the voltage profiles and cyclic performance of the Li-O_2 battery with a 3D graphene-Co_3O_4 cathode at a current density of 0.1 mA cm^{-2} and with the capacity limited to 583 mAh g^{-1} (1000 mAh g_{carbon}^{-1}). After 62 cycles the cut-off discharge voltage is still above 2.0V, showing the enhanced stability of Li-O_2 cells with the 3D graphene-Co_3O_4 cathode while the battery with 3D graphene electrode barely delivers 28 stable cycles even with the capacity cutoff of 500 mAh g^{-1}. One possible factor for this improved cycling performance is the electrode structure i.e. the intrinsically unblocked pores of the Ni foam cathode are conducive to free oxygen transport and allow easy electrolyte penetration. Another possible reason is that distinctive porous structure consisting of Co_3O_4 nanosheets grown on 3D graphene conductive channels can accommodate and degrade the insoluble discharge product efficiently, which is supported by the electrochemical impedance spectra (EIS) discussed below.

EIS at different discharge-charge stages were measured to get insight into the electrochemical performance of the 3D graphene-Co_3O_4 electrode (Fig. 5c). Compared with the initial electrode, the impedance of the cell increases dramatically after the first discharge. This is attributed to the discharge products generated in the cathode being poorly conductive. Fortunately, there is no distinct addition in the impedance values after first charge, which demonstrates that insulated discharge products are nearly completely decomposed. XPS measurement results on the products after discharge-charge further supported this reasoning, also identified discharge products on the electrode. The Li_2O_2 (55.2 eV) can be detected after 1st discharge in Fig. 5d while the peak corresponding to Li_2O_2 apparently disappeared after charge. However, after the 5th and 10th discharge, a small amount of Li_2CO_3 was generated (Fig. S2). It might be from the electrolyte decomposition.[11] Probably due to the negative impact of Li_2CO_3, Li_2O_2 was not completely degraded after the 5th and 10th charge. It is speculated that accumulation of Li_2CO_3 and incomplete decomposition of Li_2O_2 may lead to the weakened performance of Li-O_2 batteries with repeated cycles. The design of electrolyte and air electrode system that avoid efficiently accumulation of Li_2CO_3 is expected to guide further Li-O_2 battery development.

Conclusions

In summary, we have designed a 3D graphene-Co_3O_4 electrode through a two-step method that deposits graphene onto Ni foam on which are grown Co_3O_4 nanosheets. This binder-free and freestanding electrode not only inherits the unblocked porous structure of Ni foam, but also possesses uniform Co_3O_4 nanosheets interconnected with each other. The unique 3D structure and superior catalytic activity facilitates O_2 and electrolyte transport in the inner electrode and efficiently decomposes discharge products. Electrochemical evaluation reveals that the prepared electrode presents enhanced electrochemical performance with enlarged specific capacity and reduced overpotential compared with electrodes merely using a 3D graphene grown onto Ni foam. The Li-O_2 battery delivers a specific capacity of 2453 mAh g^{-1} at 0.1 mA cm^{-2} and demonstrates 62 stable cycles with 583 mAh g^{-1} (1000 mAh g_{carbon}^{-1}). As an attractive alternative method, the synthesis strategy described here may be further extended in other energy-storage device applications.

Acknowledgements

This work is financially supported by the National Natural Science Foundation of China (Grant no. 21376001) and is also supported by the Excellent Young Scholars Research Fund of Beijing Institute of Technology, contract no.2013YR1013.

Notes and references

[a] *Beijing Key Laboratory for Chemical Power Source and Green Catalysis, School of Chemical Engineering and Environment, Beijing Institute of Technology, Beijing, 100081, China, E-mail: bitkeningsun@163.com; sunwang@bit.edu.cn; Tel&Fax:0086-10-68918696*

[b] *School of Chemistry and Chemical Engineering, Queen's University, Belfast, Northern Ireland BT9 5AG, United Kingdom.*

1 P. G. Bruce, S. A. Freunberger, L. J. Hardwick and J.-M. Tarascon, *Nat. Mater.*, 2012, **11**, 19-29.
2 K. M. Abraham and Z. Jiang, *J. Electrochem. Soc.*, 1996, **143**, 1-5.
3 T. Ogasawara, A. Debart, M. Holzapfel, P. Novak and P. G. Bruce, *J. Am. Chem. Soc.*, 2006, **128**, 1390-1393.
4 J. Christensen, P. Albertus, R. S. Sanchez-Carrera, T. Lohmann, B. Kozinsky, R. Liedtke, J. Ahmed and A. Kojic, *J. Electrochem. Soc.*, 2012, **159**, R1-R30.
5 Y. Shao, F. Ding, J. Xiao, J. Zhang, W. Xu, S. Park, J.-G. Zhang, Y. Wang and J. Liu, *Adv. Fun. Mater.*, 2013, **23**, 987-1004.
6 G. Girishkumar, B. McCloskey, A. C. Luntz, S. Swanson and W. Wilcke, *J. Phys. Chem. Lett.*, 2010, **1**, 2193-2203.
7 R. Cao, J.-S. Lee, M. Liu and J. Cho, *Adv. Energy Mater.*, 2012, **2**, 816-829.
8 R. Padbury and X. Zhang, *J. Power Sources*, 2011, **196**, 4436-4444.
9 D. Capsoni, M. Bini, S. Ferrari, E. Quartarone and P. Mustarelli, *J. Power Sources*, 2012, **220**, 253-263.
10 X. Lin, L. Zhou, T. Huang and A. Yu, *J. Mater. Chem. A*, 2013, **1**, 1239-1245.
11 H.-D. Lim, H. Song, H. Gwon, K.-Y. Park, J. Kim, Y. Bae, H. Kim, S.-K. Jung, T. Kim, Y. H. Kim, X. Lepro, R. Ovalle-Robles, R. H. Baughman and K. Kang, *Energy Environ. Sci.*, 2013, **6**, 3570-3575.
12 H.-D. Lim, H. Song, J. Kim, H. Gwon, Y. Bae, K.-Y. Park, J. Hong, H. Kim, T. Kim, Y. H. Kim, X. Lepro, R. Ovalle-Robles, R. H. Baughman and K. Kang, *Angew. Chem. Int. Ed.*, 2014, **53**, 3926-3931.
13 R. Black, J.-H. Lee, B. Adams, C. A. Mims and L. F. Nazar, *Angew. Chem. Int. Ed.*, 2013, **52**, 392-396.
14 X. Ren, S. S. Zhang, D. T. Tran and J. Read, *J. Mater. Chem.*, 2011, **21**, 10118-10125.
15 J.-H. Lee, R. Black, G. Popov, E. Pomerantseva, F. Nan, G. A. Botton and L. F. Nazar, *Energy Environ. Sci.*, 2012, **5**, 9558-9565.
16 Y. Lu, Z. Wen, J. Jin, Y. Cui, M. Wu and S. Sun, *J. Solid State Electrochem.*, 2012, **16**, 1863-1868.
17 Y.-C. Lu, D. G. Kwabi, K. P. C. Yao, J. R. Harding, J. Zhou, L. Zuin and Y. Shao-Horn, *Energy Environ. Sci.*, 2011, **4**, 2999-3007.
18 J. Xiao, D. Mei, X. Li, W. Xu, D. Wang, G. L. Graff, W. D. Bennett, Z. Nie, L. V. Saraf, I. A. Aksay, J. Liu and J.-G. Zhang, *Nano Lett.*, 2011, **11**, 5071-5078.
19 X. Lin, X. Lu, T. Huang, Z. Liu and A. Yu, *J. Power Sources*, 2013, **242**, 855-859.
20 Y. Li, J. Wang, X. Li, D. Geng, R. Li and X. Sun, *Chem. Commun.*, 2011, **47**, 9438-9440.
21 H.-D. Lim, K.-Y. Park, H. Song, E. Y. Jang, H. Gwon, J. Kim, Y. H. Kim, M. D. Lima, R. O. Robles, X. Lepro, R. H. Baughman and K. Kang, *Adv. Mater.*, 2013, **25**, 1348-1352.
22 X. Hu, X. Han, Y. Hu, F. Cheng and J. Chen, *Nanoscale*, 2014, **6**, 3522-3525.
23 L. Zhang, X. Zhang, Z. Wang, J. Xu, D. Xu and L. Wang, *Chem. Commun.*, 2012, **48**, 7598-7600.
24 Y. Cao, Z. Wei, J. He, J. Zang, Q. Zhang, M. Zheng and Q. Dong, *Energy Environ. Sci.*, 2012, **5**, 9765-9768.
25 J.-J. Xu, D. Xu, Z.-L. Wang, H.-G. Wang, L.-L. Zhang and X.-B. Zhang, *Angew. Chem. Int. Ed.*, 2013, **52**, 3887-3890.
26 Y. Chen, S. A. Freunberger, Z. Peng, O. Fontaine and P. G. Bruce, *Nat. Chem.*, 2013, **5**, 489.
27 A. Debart, J. Bao, G. Armstrong and P. G. Bruce, *J. Power Sources*, 2007, **174**, 1177-1182.
28 C. S. Park, K. S. Kim and Y. J. Park, *J. Power Sources*, 2013, **244**, 72-79.
29 C. Sun, F. Li, C. Ma, Y. Wang, Y. Ren, W. Yang, Z. Ma, J. Li, Y. Chen, Y. Kim and L. Chen, *J. Mater. Chem. A*, 2014, **2**, 7188-7196.
30 R. Black, S. H. Oh, J.-H. Lee, T. Yim, B. Adams and L. F. Nazar, *J. Am. Chem. Soc.*, 2012, **134**, 2902-2905.
31 J. Xie, X. Yao, I. P. Madden, D. E. Jiang, L. Y. Chou, C. K. Tsung and D. Wang, *J. Am. Chem. Soc.*, 2014, **136**, 8903-8906.
32 Q.-c. Liu, J.-j. Xu, Z.-w. Chang and X.-b. Zhang, *J. Mater. Chem. A*, 2014, **2**, 6081-6085.
33 Y. Cui, Z. Wen and Y. Liu, *Energy Environ. Sci.*, 2011, **4**, 4727-4734.
34 K. S. Novoselov, A. K. Geim, S. V. Morozov, D. Jiang, M. I. Katsnelson, I. V. Grigorieva, S. V. Dubonos and A. A. Firsov, *Nature*, 2005, **438**, 197-200.
35 K. S. Novoselov, A. K. Geim, S. V. Morozov, D. Jiang, Y. Zhang, S. V. Dubonos, I. V. Grigorieva and A. A. Firsov, *Science*, 2004, **306**, 666-

669.
36 A. K. Geim, *Science*, 2009, **324**, 1530-1534.
37 Y. Liang, Y. Li, H. Wang, J. Zhou, J. Wang, T. Regier and H. Dai, *Nat. Mater.*, 2011, **10**, 780-786.
38 Z.-S. Wu, W. Ren, L. Wen, L. Gao, J. Zhao, Z. Chen, G. Zhou, F. Li and H.-M. Cheng, *Acs Nano*, 2010, **4**, 3187-3194.
39 S. Chen, J. Duan, J. Ran, M. Jaroniec and S. Z. Qiao, *Energy Environ. Sci.*, 2013, **6**, 3693-3699.
40 Z.-S. Wu, Y. Sun, Y.-Z. Tan, S. Yang, X. Feng and K. Muellen, *J. Am. Chem. Soc.*, 2012, **134**, 19532-19535.
41 S. Park and R. S. Ruoff, *Nat. Nanotech.*, 2009, **4**, 217-224.
42 D. A. Dikin, S. Stankovich, E. J. Zimney, R. D. Piner, G. H. B. Dommett, G. Evmenenko, S. T. Nguyen and R. S. Ruoff, *Nature*, 2007, **448**, 457-460.
43 K. S. Kim, Y. Zhao, H. Jang, S. Y. Lee, J. M. Kim, K. S. Kim, J.-H. Ahn, P. Kim, J.-Y. Choi and B. H. Hong, *Nature*, 2009, **457**, 706-710.
44 Z. Chen, W. Ren, L. Gao, B. Liu, S. Pei and H.-M. Cheng, *Nat. Mater.*, 2011, **10**, 424-428.
45 X. Cao, Y. Shi, W. Shi, G. Lu, X. Huang, Q. Yan, Q. Zhang and H. Zhang, *Small*, 2011, **7**, 3163-3168.
46 Q. K. Yu, J. Lian, S. Siriponglert, H. Li, Y. P. Chen and S. S. Pei, *Appl. Phys. Lett.*, 2008, **93**, 113103.
47 X. Li, W. Cai, J. An, S. Kim, J. Nah, D. Yang, R. Piner, A. Velamakanni, I. Jung and E. Tutuc, *Science*, 2009, **324**, 1312-1314.
48 A. Reina, X. Jia, H. John, D. Nezich, H. Son, V. Bulovic, M. S. Dresselhaus and J. Kong, *Nano Lett.*, 2009, **9**, 30–35.
49 Y. Li, B. Tan and Y. Wu, *Chem. Mater.*, 2008, **20**, 567-576.
50 T. Yu, Y. W. Zhu, X. J. Xu, Z. X. Shen, P. Chen, C. T. Lim, J. T. L. Thong and C. H. Sow, *Adv. Mater.*, 2005, **17**, 1595-1599.
51 G. Wang, X. Shen, J. Horvat, B. Wang, H. Liu, D. Wexler and J. Yao, *J. Phys. Chem. C*, 2009, **113**, 4357-4361.
52 C. Yuan, L. Yang, L. Hou, L. Shen, F. Zhang, D. Li and X. Zhang, *J. Mater. Chem.*, 2011, **21**, 18183-18185.
53 G. Zhao, Z. Xu and K. Sun, *J. Mater. Chem. A*, 2013, **1**, 12862-12867.